Automatic Identification of the Pectoral Muscle in Mammograms

R. J. Ferrari, *Member, IEEE*, R. M. Rangayyan*, *Fellow, IEEE*, J. E. L. Desautels, R. A. Borges, and A. F. Frère

***Abstract*—The pectoral muscle represents a predominant density region in most medio-lateral oblique (MLO) views of mammograms; its inclusion can affect the results of intensity-based image processing methods or bias procedures in the detection of breast cancer. Local analysis of the pectoral muscle may be used to identify the presence of abnormal axillary lymph nodes, which may be the only manifestation of occult breast carcinoma. We propose a new method for the identification of the pectoral muscle in MLO mammograms based upon a multiresolution technique using Gabor wavelets. This new method overcomes the limitation of the straight-line representation considered in our initial investigation using the Hough transform. The method starts by convolving a group of Gabor filters, specially designed for enhancing the pectoral muscle edge, with the region of interest containing the pectoral muscle. After computing the magnitude and phase images using a vector-summation procedure, the magnitude value of each pixel is propagated in the direction of the phase. The resulting image is then used to detect the relevant edges. Finally, a post-processing stage is used to find the true pectoral muscle edge. The method was applied to 84 MLO mammograms from the Mini-MIAS (Mammographic Image Analysis Society, London, U.K.) database. Evaluation of the pectoral muscle edge detected in the mammograms was performed based upon the percentage of false-positive (FP) and false-negative (FN) pixels determined by comparison between the numbers of pixels enclosed in the regions delimited by the edges identified by a radiologist and by the proposed method. The average FP and FN rates were, respectively, 0.58% and 5.77%. Furthermore, the results of the Gabor-filter-based method indicated low Hausdorff distances with respect to the hand-drawn pectoral muscle edges, with the mean and standard deviation being 3.84 ± 1.73 mm over 84 images.**

***Index Terms*—Breast cancer, Gabor wavelets, Hough transform, mammography, pectoral muscle.**

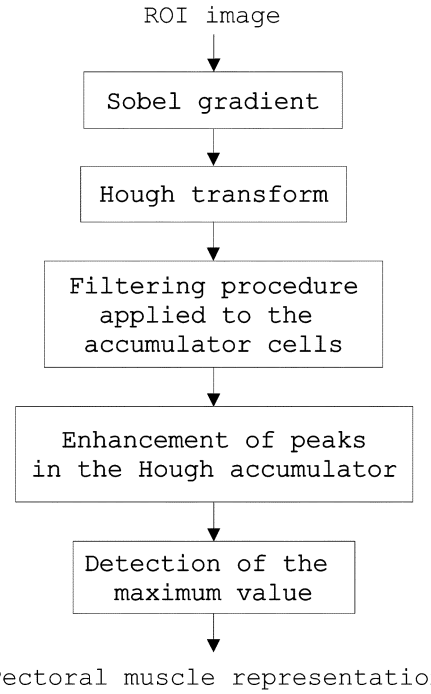

Fig. 1. Flow chart of the procedure for identification of the pectoral muscle by using the Hough transform (Method 1).

I. Introduction

THE pectoral muscle represents a predominant density region in most medio-lateral oblique (MLO) views of mammograms, and can affect the results of image processing methods. Intensity-based methods, for example, can present poor performance when applied to differentiate dense structures such as the fibro-glandular disc or small suspicious masses, since the pectoral muscle appears at approximately the same density as the dense tissues of interest in the image. The inclusion of the pectoral muscle in the image data being processed could also bias the detection procedures. Another important need to identify the pectoral muscle lies in the possibility that the local information of its edge, along with an internal analysis of its region, may be used to identify the presence of abnormal axillary lymph nodes, which may be the only manifestation of occult breast carcinoma [1].

Manuscript received June 10, 2003; revised October 23, 2003. This work was supported in part by grants from Coordenação de Aperfeiçoamento de Pessoal de Ensino Superior (CAPES) and Fundação de Amparo à Pesquisa do Estado de São Paulo (FAPESP), Brazil; in part by the Alberta Heritage Foundation for Medical Research (AHFMR), Alberta, Canada; and in part by the Natural Sciences and Engineering Research Council (NSERC) of Canada. The Associate Editor responsible for coordinating the review of this paper and recommending its publication was N. Karssemeijer. *Asterisk indicates corresponding author.*

R. J. Ferrari is with the Department of Electrical and Computer Engineering, University of Calgary, Calgary, AB T2N 1N4, Canada and also with the Department of Electrical Engineering, University of São Paulo, São Carlos, São Paulo, Brazil, 13560-250 (e-mail: ricardof@sel.eesc.sc.usp.br).

*R. M. Rangayyan is with the Department of Electrical and Computer Engineering, University of Calgary, Calgary, AB T2N 1N4, Canada (e-mail: ranga@enel.ucalgary.ca) and also with the Department of Radiology, University of Calgary, Calgary, AB T2N 1N4, Canada.

J. E. L. Desautels is with the Department of Electrical and Computer Engineering, University of Calgary, Calgary, AB T2N 1N4, Canada and also with Screen Test Alberta, Calgary, AB T2P 3G9, Canada.

R. A. Borges is with the Nucleus of Science and Technology, University of Mogi das Cruzes, Mogi das Cruzes, São Paulo, Brazil 08780-911 and also with Mogimagem, Mogi das Cruzes, São Paulo, Brazil 08710-630.

A. F. Frère is with the Nucleus of Science and Technology, University of Mogi das Cruzes, Mogi das Cruzes, São Paulo, Brazil 08780-911 and also with the Department of Electrical Engineering, University of São Paulo, São Carlos, São Paulo, Brazil, 13560-250.

Digital Object Identifier 10.1109/TMI.2003.823062

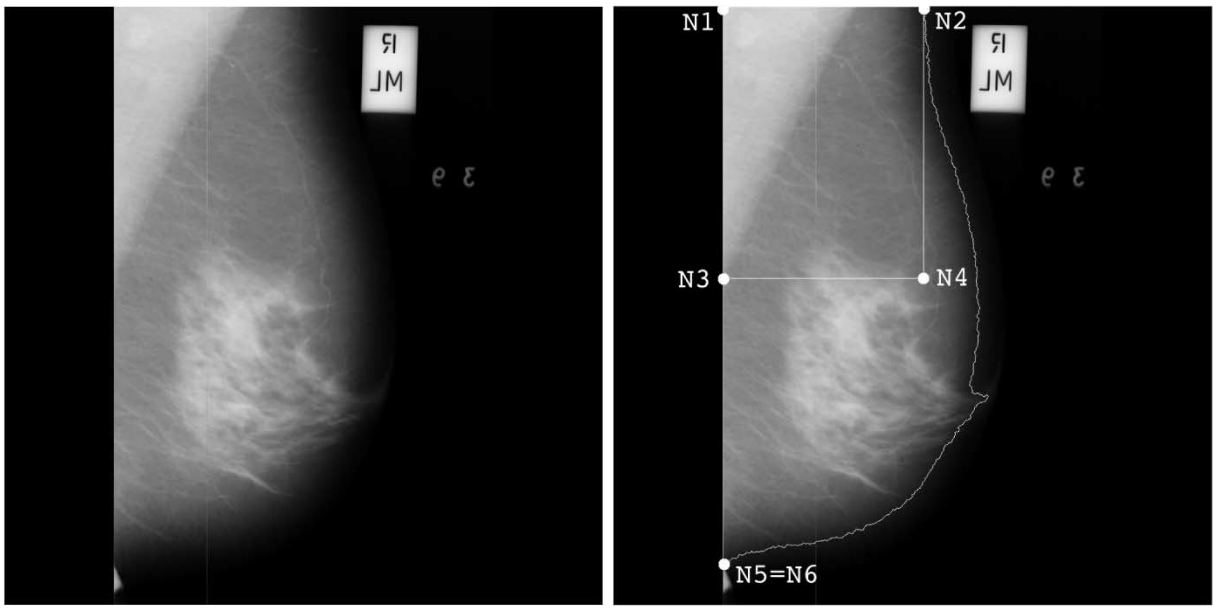

Fig. 2. (a) Original image mdb042 from the Mini-MIAS database [7]. (b) Approximate boundary of the breast along with the control points N1 to N6 (automatically determined) used to limit the region of interest (rectangle marked) for the detection of the pectoral muscle.

Only a few works have been presented in the literature to address this problem. Karssemeijer [2] used the Hough transform and a set of threshold values applied to the accumulator cells in order to detect the pectoral muscle. Aylward *et al.* [3] used their gradient magnitude ridge traversal algorithm at small scale, and then solved the resulting multiple edges via a voting scheme in order to segment the pectoral muscle region. In an earlier publication [4], we presented a technique to detect the pectoral muscle based upon the Hough transform, which was a modification of the method proposed by Karssemeijer [2]. However, the hypothesis of a straight line for the representation of the pectoral muscle is not always correct, and may impose limitations on subsequent stages of image analysis.

The method proposed in this paper to identify the pectoral muscle in MLO views is based upon the Gabor wavelet representation proposed by Manjunath and Ma [5]. This method overcomes the limitation of the straight-line representation mentioned above.

The paper is organized as follows: Section II presents our initial work (Method 1) for the detection of the pectoral muscle using the Hough transform. Section III presents the new proposed method using Gabor wavelets (Method 2). The characteristics of the database used in this paper are presented in Section IV. The protocol used for the evaluation of the results is presented in Section V, followed by the results and discussion in Section VI. Conclusions are presented in Section VII.

II. Method 1: Identification of the Pectoral Muscle Using the Hough Transform

Our initial method to identify the pectoral muscle [4], summarized in the flow chart in Fig. 1, starts by automatically identifying an appropriate region of interest (ROI) containing the pectoral muscle, as shown in Fig. 2. To begin with, an approximate breast contour delimiting the control points is obtained by using our method for the detection of the skin-air boundary [4]. Briefly, this method starts by applying a binarization procedure to the image, and the chain-code algorithm is used to find an approximate breast contour. The identification of the true breast boundary is performed by using the approximate contour as the input to an active contour model algorithm specially tailored for this purpose. The six control points N1–N6 used to define the ROI are determined as: N1: top-left corner pixel of the

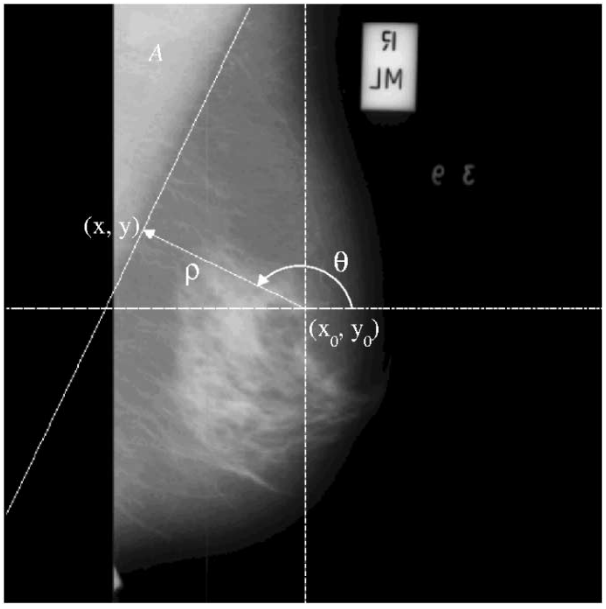

Fig. 3. Coordinate system used to compute the Hough transform. The pectoral muscle line detected is also shown.

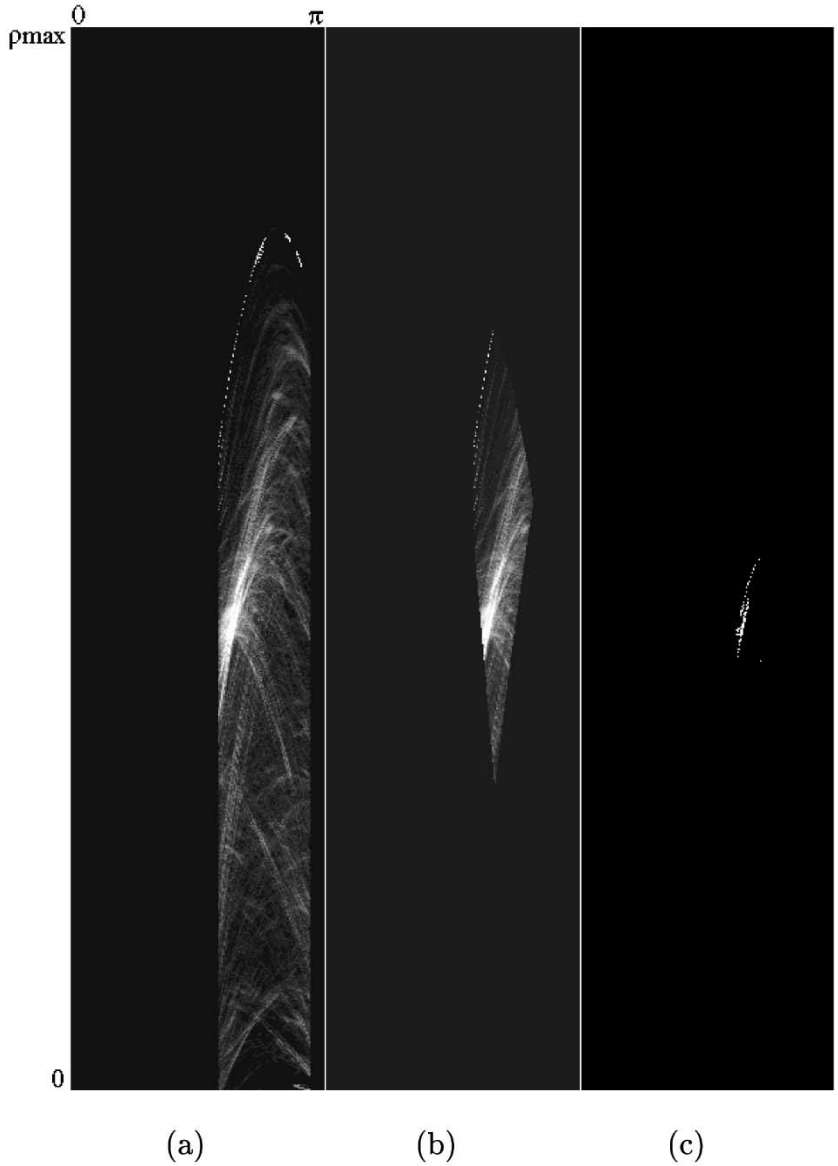

Fig. 4. Hough accumulator cells obtained at different stages of the procedure used to determine the pectoral muscle line. The contrast of the images has been modified for the sake of improved visualization. (a) Accumulator cells obtained by using the constraint $|\phi_{x,y} - \theta| < 2^\circ$ and $(120^\circ \leq \theta \leq 170^\circ)$. (b) Accumulator cells after removing the lines intercepting the top of the image outside the region defined by the control points N1-N2 (see Fig. 3). (c) Accumulator after applying the multiplicative factor $\alpha = (\mu/\sigma^2)A \Big|_{\theta,\rho}$. The parameter pair (ρ, θ) of the cell presenting the maximum value is used to define the pectoral line.

boundary loop; N5: lowest pixel on the left edge of the boundary loop; N3: mid-point between N1 and N5; N2: the farthest point on the boundary from N5, in terms of the Euclidean distance through the breast (if this point is not located on the upper edge of the mammogram, it is projected vertically to the upper edge); N4: the point that completes a rectangle with N1, N2, and N3 (not necessarily on the boundary loop); N6: the farthest point on the boundary loop from N1. In the case of the mammogram in Fig. 2, the points N5 and N6 have coincided.

The ROI is defined by the rectangular region delimited by the points N1, N2, N3, and N4, as illustrated in Fig. 2. Although, in some cases, this region may not include the total length of the pectoral muscle, the portion of the muscle present is adequate to define a straight line to represent its edge. By limiting the size of the ROI as described above, we minimize the possibilities of other linear structures that may be present in the fibro-glandular disc biasing the representation of the pectoral muscle edge.

The method, which is based on the Hough transform [6], is a modification of the method proposed by Karssemeijer [2]. Differing from Karssemeijer's method, we do not use any threshold value in order to reduce the number of unlikely pectoral lines. Instead, we use geometric and anatomical constraints, which are summarized as follows:

1) The pectoral muscle is considered to be a straight line limited to an angle θ between 120° and 170°, with the angle computed as indicated in Fig. 3. Mammograms of right breasts are flipped (mirrored) before performing pectoral muscle detection.
2) The pectoral line intercepts the line segment N1-N2, as indicated in Fig. 2.

3) The pectoral line is present, in partial or total length, in the ROI defined as the rectangular region delimited by the points N1, N2, N3, and N4, as illustrated in Fig. 2.
4) After lowpass filtering (convolution with a Gaussian kernel), the pectoral muscle appears on mammograms as a dense region with nearly homogeneous gray-level values.

After selecting the ROI, a Gaussian filter with $\sigma_x = \sigma_y = 4$ pixels is used to smooth the ROI in order to remove high-frequency noise in the image. (At this stage, the images are of size 256×256 pixels at a resolution of 800 μm/pixel.) The Hough transform is then applied to the Sobel gradient of the ROI [6] to detect the edge of the pectoral muscle. The representation of a straight line for the Hough transform computation is specified as

$$\rho = (x - x_0)\cos\theta + (y - y_0)\sin\theta \tag{1}$$

where (x_0, y_0) is the origin of the coordinate system of the image located at the center of the image, and ρ and θ represent, respectively, the distance and angle between (x_0, y_0) and the coordinates (x, y) of the pixel being analyzed, as illustrated in Fig. 3. The Hough accumulator is quantized to 45 bins of 4° each by using the constraint $|\phi_{x,y} - \theta| < 2°$, where $\phi_{x,y}$ is the orientation of the Sobel gradient of the pixel (x, y). In this paper, the accumulator cells are incremented using the magnitude of the gradient instead of unit increments; thus, pixels with a strong gradient will have larger weights. Only values of θ in the range $120° \leq \theta \leq 170°$ are considered in the analysis since the pectoral muscle of the mammogram is always positioned on the left-hand side of the image before computing the Hough transform (see Fig. 3).

After computing the accumulator cell values in the Hough space, we apply a filtering procedure to eliminate all lines (pairs of parameters ρ and θ) unlikely to represent the pectoral muscle. In this procedure, all lines intercepting the top of the image outside the N1-N2 line segment (see Fig. 2) or with slopes outside the range [120°, 170°] are removed. (In this paper, the x axis corresponds to zero degree and the chest wall is positioned on the left-hand side; see Fig. 3.) Each remaining accumulator cell is also multiplied by the factor

$$\alpha = \frac{\mu}{\sigma^2} A \Big|_{\theta,\rho} \tag{2}$$

where μ and σ^2 are, respectively, the mean and the variance of the gray-level values in the area A of the pectoral muscle (see Fig. 3) defined by the straight line specified by the parameters θ and ρ. This procedure was applied in order to enhance the Hough transform peaks which define regions with the property stated in Item 4 of the list provided earlier in this section. The weight related to the area was designed to differentiate the true pectoral muscle from the pectoralis minor; the latter could present a higher contrast than the former in some cases, albeit enclosing a smaller area than the former.

Finally, the parameters ρ and θ of the accumulator cell with the maximum value are taken to represent the pectoral muscle line. Fig. 4 shows the Hough accumulator cells resulting for the different stages of the procedure described above for the mammogram in Fig. 2(a). The pectoral muscle line detected for the mammogram in Fig. 2(a) is shown in Fig. 3.

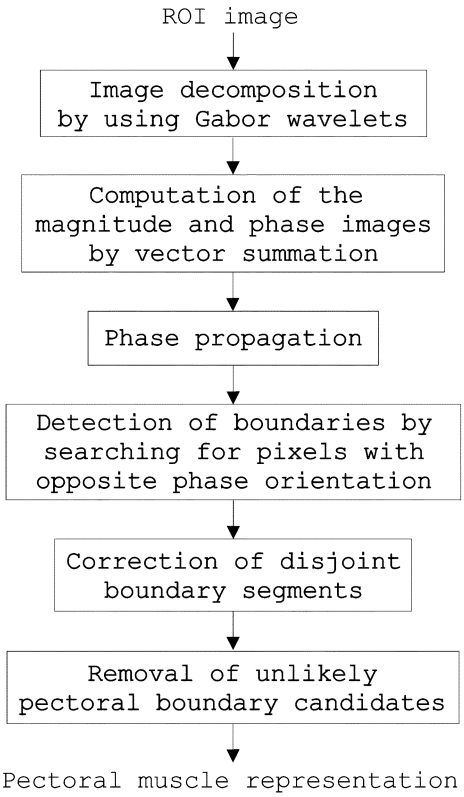

Fig. 5. Flow chart of the procedure for identification of the pectoral muscle by using Gabor wavelets (Method 2).

III. Method 2: Identification of the Pectoral Muscle Using Gabor Wavelets

In our improved method, summarized by the flow chart in Fig. 5, a bank of Gabor filters is designed to enhance the directional, piecewise-linear structures that are present in the ROI containing the pectoral muscle. Fig. 6(a) illustrates the image mdb028 from the Mini-MIAS database [7]; Fig. 6(b) shows the ROI used for detection of the pectoral muscle, defined automatically as the rectangle formed by the chest wall as the left-hand edge, and a vertical line through the upper-most point on the skin-air boundary drawn along the entire height of the mammogram as the right-hand edge. Differing from Method 1, described in Section II, the ROI is defined to contain the entire pectoral muscle region, since we are not using a straight-line representation. Decomposition of the ROI to components with different scale and orientation is performed by convolution of the ROI image with a bank of tunable Gabor filters. The magnitude and phase components of the filtered images are then combined and used as input to a post-processing stage, as described in the following sections.

A. Design of the Gabor Wavelets

A two-dimensional (2-D) Gabor function is a Gaussian modulated by a complex sinusoid, which can be specified by the frequency of the sinusoid W and the standard deviations σ_x and σ_y of the Gaussian envelope as [5], [8]

$$\psi(x, y) = \frac{1}{2\pi\sigma_x\sigma_y} \exp\left[-\frac{1}{2}\left(\frac{x^2}{\sigma_x^2} + \frac{y^2}{\sigma_y^2}\right)\right] \exp(j2\pi W x). \tag{3}$$

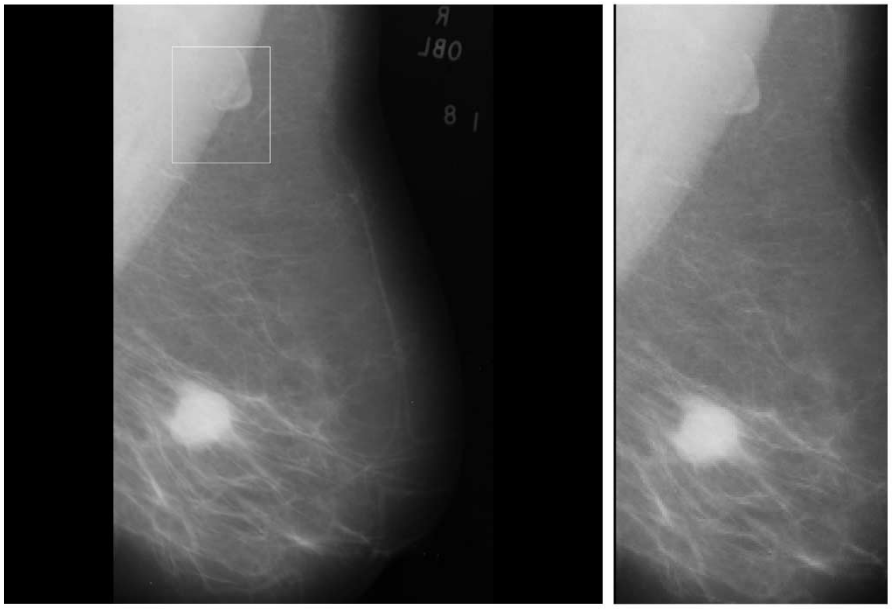

(a) (b)

Fig. 6. (a) Original image mdb028 and (b) the ROI used to search for the pectoral muscle region, defined by the chest wall on the left and a vertical line through the upper-most point on the skin-air boundary drawn along the entire height of the mammogram on the right. The box drawn in (a) is not related to the ROI in (b).

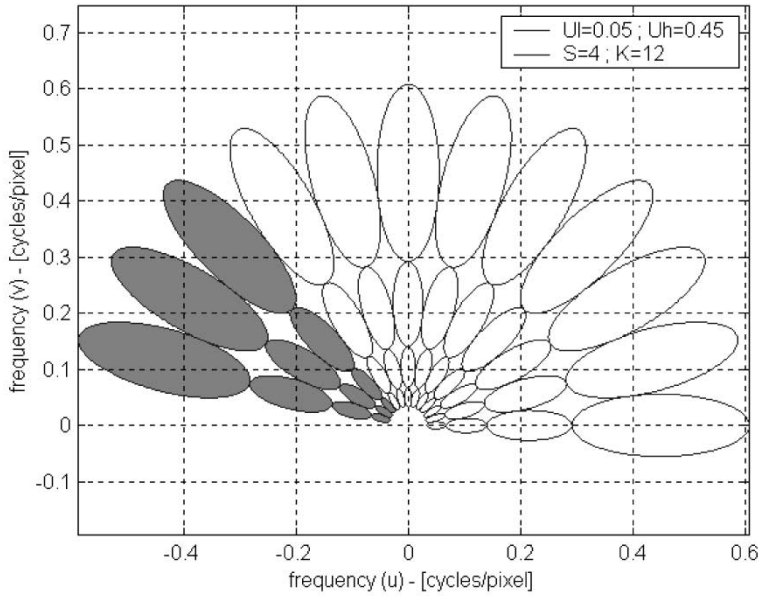

Fig. 7. Bank of Gabor filters designed in the frequency domain. Each ellipse represents the range of the corresponding filter response from 0.5 to 1.0 in squared magnitude (only one half of the response is shown for each filter). The sampling of the frequency spectrum can be adjusted by changing the U_l, U_h, S, and K parameters of the Gabor representation. Only the filters shown shaded were used to enhance the directional piece-wise linear structures present in the ROI images. The frequency axes are normalized.

Gabor wavelets are obtained by dilation and rotation of $\psi(x,y)$ as in (3) by using the generating function

$$\begin{aligned}\psi_{m,n}(x,y) &= a^{-m}\psi(x',y'),\ a>1,\ m,n=\text{integers}\\ x' &= a^{-m}[(x-x_0)\cos\theta+(y-y_0)\sin\theta]\\ y' &= a^{-m}[-(x-x_0)\sin\theta+(y-y_0)\cos\theta] \quad (4)\end{aligned}$$

where (x_0,y_0) is the center of the filter in the spatial domain, $\theta=n\pi/K$, K is the number of orientations desired, and m and n indicate the scale and orientation, respectively. The Gabor filters used in this paper may be expressed in the frequency domain as

$$\begin{aligned}&\Psi(u,v)\\ &\quad=\frac{1}{2\pi\sigma_u\sigma_v}\exp\left\{-\frac{1}{2}\left[\frac{(u-W)^2}{\sigma_u^2}+\frac{v^2}{\sigma_v^2}\right]\right\}\ \text{for}\ (u,v)\neq(0,0)\\ &\quad=0\ \text{for}\ (u,v)=(0,0) \quad (5)\end{aligned}$$

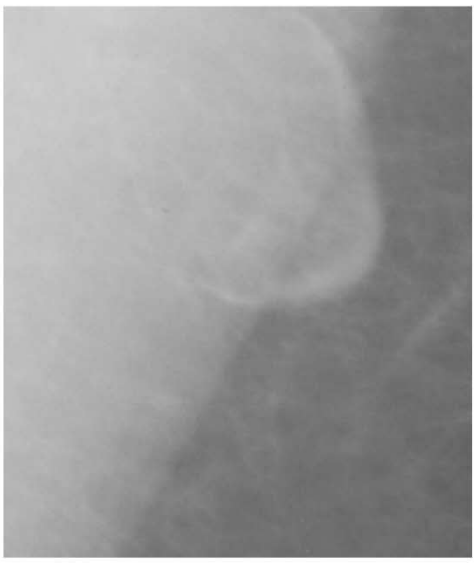

(a)

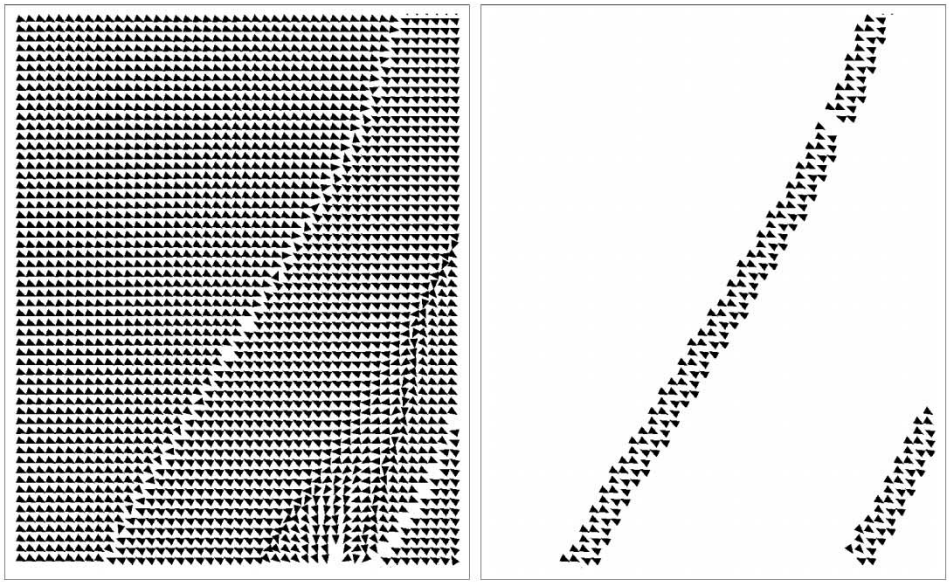

(b) (c)

Fig. 8. (a) Region indicated in Fig. 6(a) containing part of the pectoral muscle edge. Images (b) and (c) show the edge-flow map before and after propagation. Each arrowhead represents the direction of the edge-flow vector at the corresponding position in the image.

where $\sigma_u = 1/(2\pi\sigma_x)$ and $\sigma_v = 1/(2\pi\sigma_y)$. The design strategy used is to project the filters so as to ensure that the half-peak magnitude supports of the filter responses in the frequency spectrum touch one another, as shown in Fig. 7. By doing this, it can be ensured that the filters will capture the maximum information with minimum redundancy. In order for the designed bank of Gabor filters to be a family of admissible 2-D Gabor wavelets [9], the filters $\psi(x, y)$ must satisfy the admissibility condition of finite energy [10], which implies that their Fourier transforms are pure bandpass functions having zero response at d.c.. This condition was achieved by setting the d.c. gain of each filter as $\Psi(0,0) = 0$, which makes the filters not to respond to regions with constant intensity.

The following formulas provide the filter parameters σ_u and σ_v:

$$
\begin{aligned}
a &= \left(\frac{U_h}{U_l}\right)^{1/(S-1)} \\
\sigma_u &= \frac{(a-1)U_h}{(a+1)\sqrt{2\ln 2}} \\
\sigma_v &= \frac{\tan(\frac{\pi}{2K})\left[U_h - (\frac{\sigma_u^2}{U_h})2\ln 2\right]}{\sqrt{2\ln 2 - \frac{(2\ln 2)^2\sigma_u^2}{U_h^2}}}
\end{aligned}
\tag{6}
$$

where U_l and U_h denote the lower and upper center frequencies of interest; the K and S parameters are, respectively, the

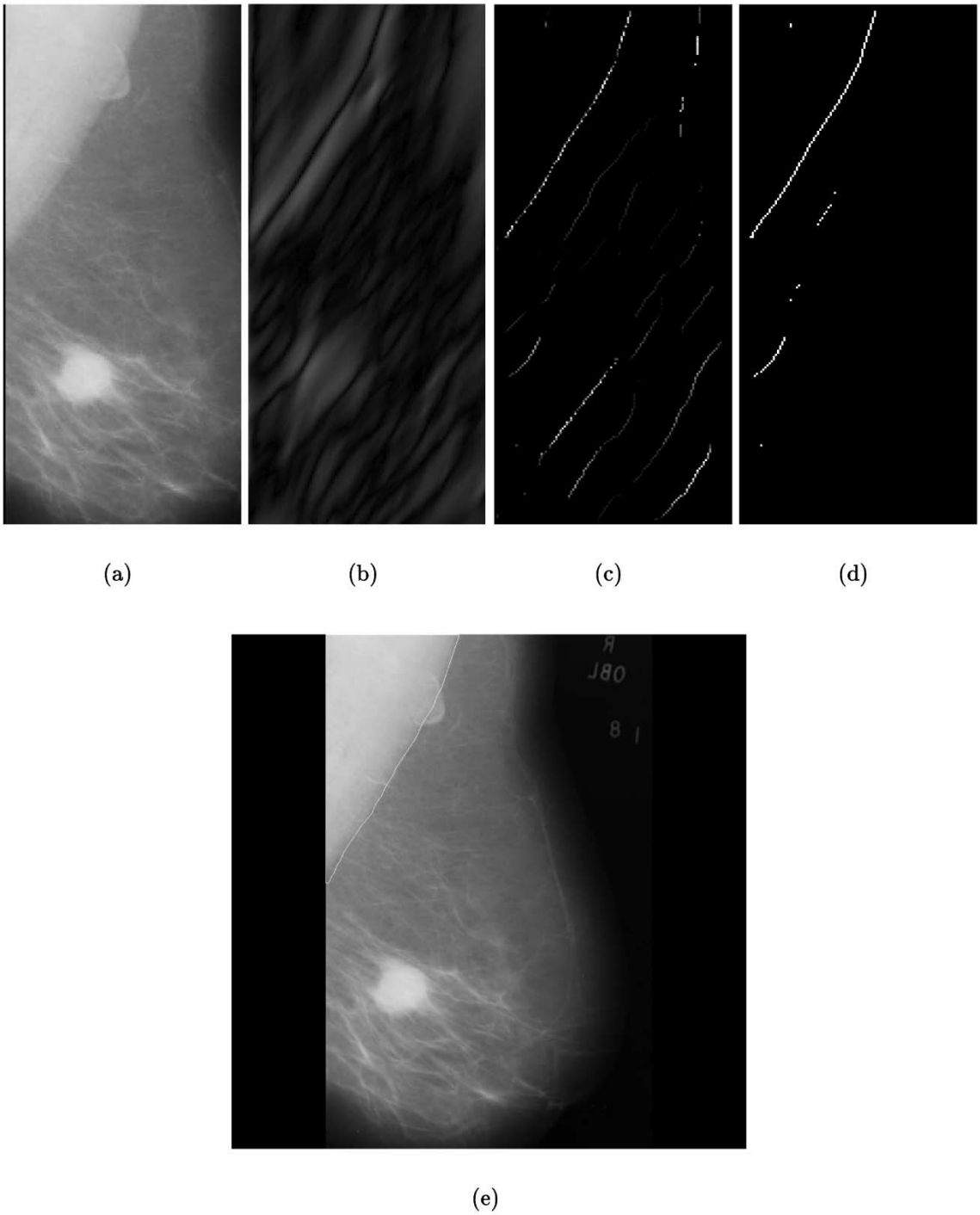

Fig. 9. Result of each stage of the method for detection of the pectoral muscle edge. (a) ROI used to search for the pectoral edge. (b) Image magnitude resulting after application of the Gabor filters and vector summation; the contrast was modified by gamma correction (with $\mathrm{gamma} = 0.7$) for the sake of improved visualization. (c)–(d) Image resulting before and after the post-processing stage. (e) Final boundary.

number of orientations and the number of scales in the desired multiresolution decomposition procedure; $m = 0, 1, \ldots, S-1$; and the sinusoid frequency W is set equal to U_h, such that the magnitude responses of the filters span the full spectrum of the image as shown in Fig. 7.

In this paper, we are only interested in image analysis without the requirement of exact reconstruction (synthesis) of the image. Therefore, instead of using the wavelet coefficients, we have used the magnitude of the filter response, computed as

$$a_{m,n} = \left| f(x,y) * \psi^{\mathrm{even}}_{m,n}(x,y) \right| \tag{7}$$

where $\psi^{\mathrm{even}}_{m,n}(x,y)$ indicates the even-symmetric part of the complex Gabor filter, $f(x,y)$ is the ROI being filtered, and $*$ represents the convolution operator. The phase and magnitude

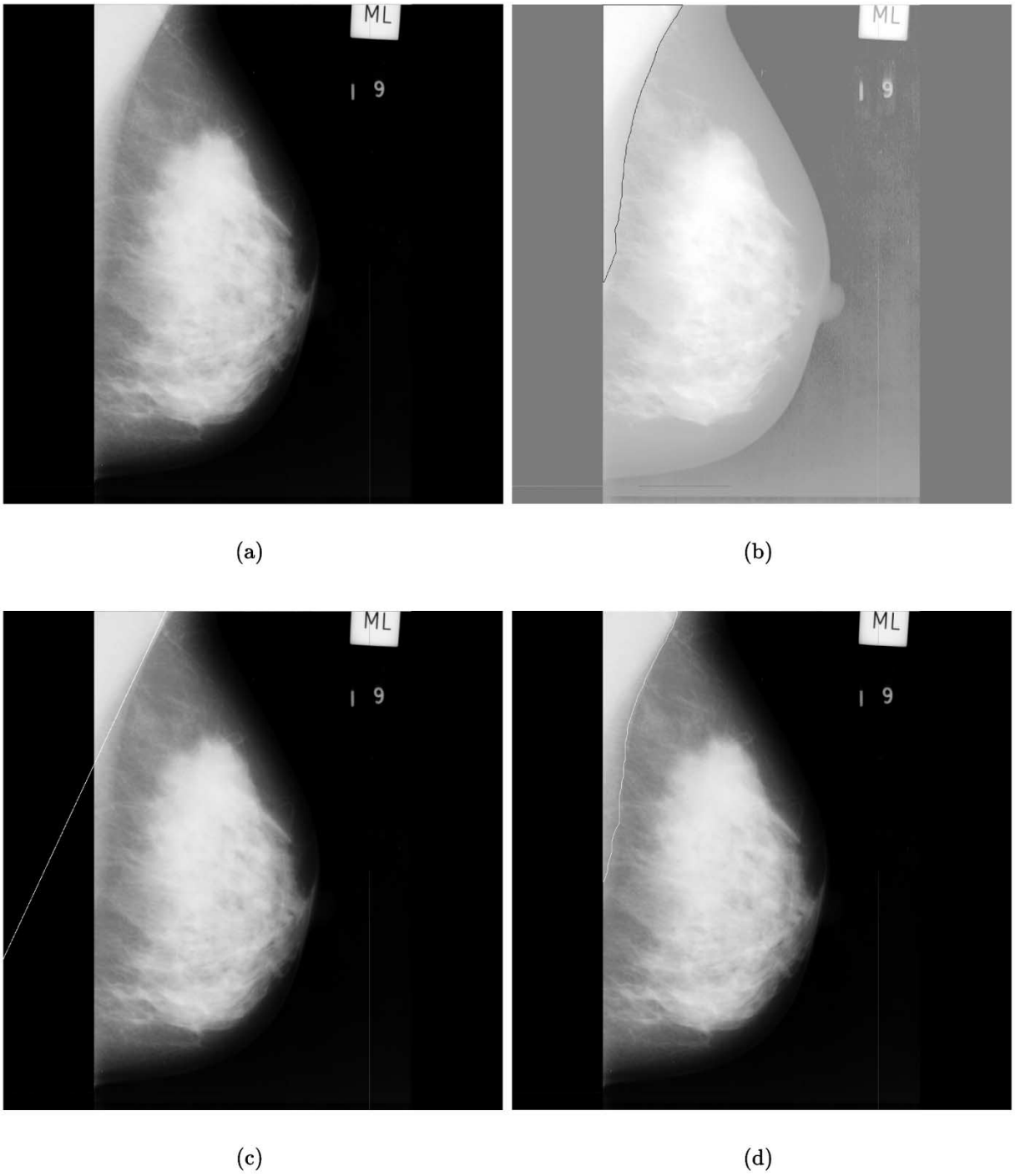

Fig. 10. Results obtained for the image mdb003. (a) Original image. (b) Hand-drawn pectoral muscle edge superimposed on the histogram-equalized image. (c) and (d) Pectoral muscle edges detected, respectively, by Method 1 (using the Hough transform) and by Method 2 (using Gabor filters), superimposed on the original image.

images, indicating the local orientation, are composed by vector summation of the K filtered images ([11, chapter 11]).

The parameters U_l and U_h permit specification of the range of the frequency spectrum to be used for multiresolution analysis. The choice of the number of scales (S) and orientations (K) used in this paper for detecting the pectoral muscle is based upon the resolution required for detecting oriented information with high selectivity [12], [13]. We have defined the Gabor filter parameters as follows: $U_l = 0.05$, $U_h = 0.45$, $S = 4$, and $K = 12$. This set of parameters provides 48 filters that span the frequency spectrum as indicated in Fig. 7.

The spatial-frequency bandwidths of the simple and complex cells in mammalian visual systems have been found to range from 0.5 to 2.5 octaves, clustering around 1.2 octaves and 1.5 octaves, and their angular bandwidth is expected to be smaller than 30° [13], [14]. The Gabor representation used in this paper provides a frequency bandwidth of approximately one octave and angular bandwidth of 15° [8]. These parameters, as well as

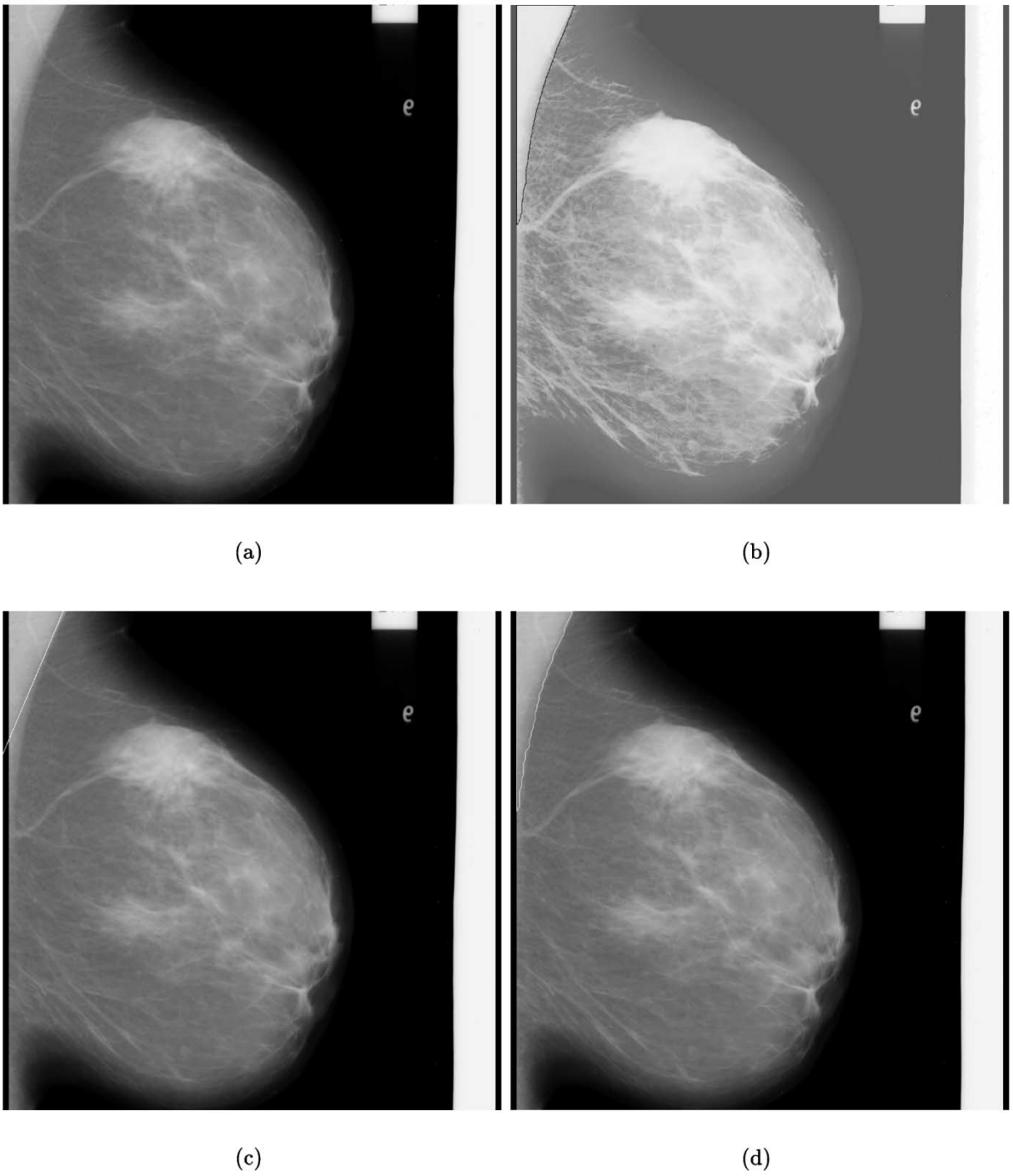

Fig. 11. Results obtained for the image mdb150. (a) Original image. (b) Hand-drawn pectoral muscle edge superimposed on the histogram-equalized image. (c) and (d) Pectoral muscle edges detected, respectively, by Method 1 (using the Hough transform) and by Method 2 (using Gabor filters), superimposed on the original image.

the observations of Manjunath and Ma [5] and Daugman [13], suggest the use of 48 Gabor filters with 12 orientations and four scales ($S = 4$) to span the full range of the spectrum, as illustrated in Fig. 7.

In this paper, all images are MLO views, and are initially oriented so that the chest wall is positioned on the left-hand side. According to Cardenosa [15, pp. 54-55], in MLO views, "the pectoral muscle should be seen to the level of the nipple," and "if the pectoral muscle edge is concave, parallel to the edge of the film, or triangular, the breast is not positioned optimally." (Unfortunately, some of the mammograms in the MIAS database do not satisfy these criteria.) Based upon these observations, the pectoral muscle edge in correctly acquired MLO views could be expected to be located within the angular range of about 30° – 80°. (Here, the orientation of the pectoral muscle edge is defined as the angle between the horizontal line and an imaginary straight line representing the pectoral muscle edge.) For this reason, we used Gabor filters with the central orientation of

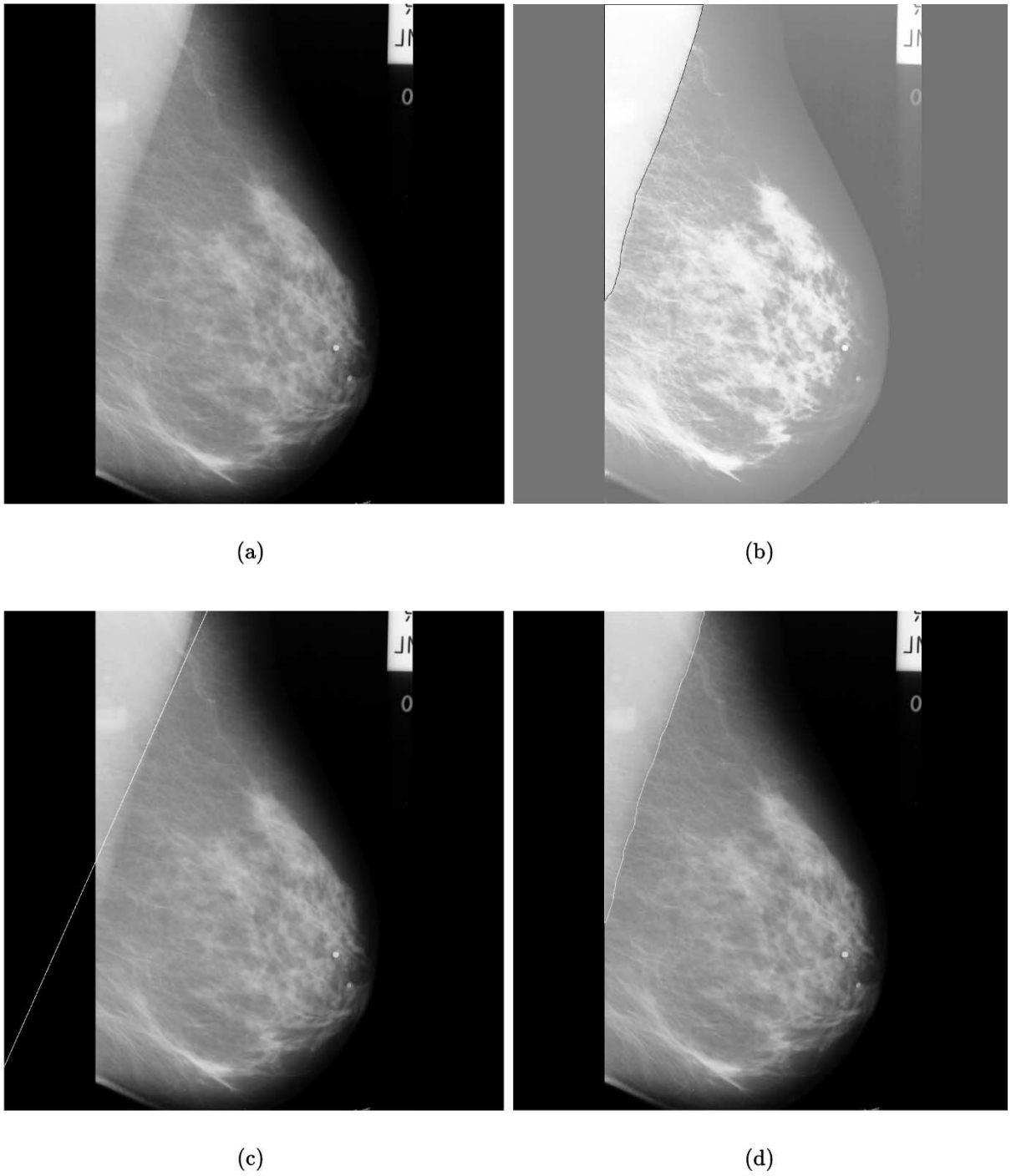

Fig. 12. Results obtained for the image mdb008. (a) Original image. (b) Hand-drawn pectoral muscle edge superimposed on the histogram-equalized image. (c) and (d) Pectoral muscle edges detected, respectively, by Method 1 (using the Hough transform) and by Method 2 (using Gabor filters), superimposed on the original image.

their responses in the image domain at 45°, 60°, and 75°; the corresponding frequency-domain responses are shown shaded in Fig. 7. Observe that the filters have a half-response angular bandwidth of 15° about the central orientations listed above.

B. Post-Processing and Pectoral Muscle Edge Detection

After computing the phase and magnitude images by vector summation, we detect relevant edges in the ROI by using an algorithm proposed by Ma and Manjunath [16] for edge-flow propagation (see Algorithm 1). However, in this paper, the magnitude $A(x, y)$ and phase $\phi(x, y)$ at each image location (x, y) are used to represent the edge-flow vector instead of using a predictive coding model as initially proposed by Ma and Manjunath. The phase at each point in the image is propagated until it reaches a location where two opposite directions of flow encounter each other. Fig. 8(b) and (c) illustrate an example of the orientation map before and after applying the edge-flow propagation procedure.

Algorithm 1 Algorithm for edge-flow propagation proposed by Ma and Manjunath **[16]**, and used in this paper to propagate the vectors resulting from the vector summation of the Gabor-filtered images.

1. Set $n = 0$ and $\vec{F}_0(x,y) = [A(x,y)\cdot\cos\phi(x,y), A(x,y)\cdot\sin\phi(x,y)]$.
2. Set the edge-flow vector $\vec{F}_{n+1}(x,y)$ at iteration $n+1$ to zero.
3. At each image location (x,y), identify the neighbor (x',y') which has the same direction θ of the edge-flow vector $\vec{F}_n(x,y)$. The direction θ is computed as $\theta = \arctan\{(y'-y)/(x'-x)\}$.
4. If $\vec{F}_n(x',y')\bullet\vec{F}_n(x,y) > 0$, where the symbol $\bullet$ indicates the dot-product operation, then $\vec{F}_{n+1}(x',y') = \vec{F}_{n+1}(x',y') + \vec{F}_n(x,y)$ else $\vec{F}_{n+1}(x,y) = \vec{F}_{n+1}(x,y) + \vec{F}_n(x,y)$.
5. If nothing has been changed then stop iterating else go to Step 2 and repeat the procedure.

After propagating the edge-flow vector, the boundary candidates for the pectoral muscle are obtained by identifying locations that have nonzero edge-flow coming from two opposite directions. Weak edges are eliminated by thresholding the ROI image with a threshold value of 10% of the maximum gray-level value in the ROI. Fig. 9 shows images resulting from each stage of the procedure for pectoral muscle detection.

In order to connect disjoint boundary segments that are usually present in the image after the edge-flow propagation step, a half-elliptical neighborhood is defined with its center located at each boundary pixel being processed. The half ellipse is adjusted to be proportional to the length of the contour, with $R_1 = 0.2C_{\text{len}}$, and $R_2 = 5$ pixels (where R_1 and R_2 are, respectively, the major and minor axes of the half ellipse, and C_{len} is the length of the boundary), with its major axis oriented along the direction of the contour line. If an ending or a starting pixel of an unconnected line segment is found in the defined neighborhood, it is connected by using a simple linear interpolation technique. The iterative method stops when all disjoint lines are connected; this procedure took only 5 – 20 iterations with the images used in this paper. Next, false edges which may result in the filtered images due to structures inside the fibro-glandular disc or due to the filtering process [see Fig. 9(c)–(d)] are removed by checking either if the shortest distances of their limiting points from the top and left edges of the ROI are greater than 30% of their lengths, or if the straight line having the same slope as the pectoral muscle edge candidate intercepts outside the top and left limits of the ROI. Finally, the largest line in the ROI is defined as the pectoral muscle edge, subject to a minimum length limit of 10 pixels (8 mm).

IV. Database

A total of 84 images, randomly chosen from the Mammographic Image Analysis Society, London, U.K. (Mini-MIAS) [7], were used in this paper. All images are MLO views with 200-μm sampling interval and 8-bit gray-level quantization. For reduction of processing time, all images were down-sampled with a fixed sampling distance so that the original images corresponding to the matrix size of 1024×1024 pixels were transformed to 256×256 pixels. All results obtained with the down-sampled images were mapped to the original 1024×1024 mammograms for subsequent analysis and display.

TABLE I
Mean (and Standard Deviation) Values of the FP and FN Pixels as Well as Hausdorff Distances Obtained for the Results of Methods 1 and 2 With 84 Images

Method	1 - Hough	2 - Gabor
Analysis of area enclosed:		
FP $\pm\sigma$	$1.98 \pm 6.09\%$	$0.58 \pm 4.11\%$
FN $\pm\sigma$	$25.19 \pm 19.14\%$	$5.77 \pm 4.83\%$
# images with (FP and FN) $< 5\%$	10	45
# images with $5\% <$ (FP and FN) $< 10\%$	8	22
# images with (FP and FN) $> 10\%$	66	17
Hausdorff distance (mm):	7.08 ± 5.26	3.84 ± 1.73

V. Protocol for Evaluation of the Results

The results obtained from both Methods 1 and 2 were evaluated in consultation with two radiologists experienced in mammography (JELD and RAB). The test images were displayed on a computer monitor (19″ diagonal size and dot pitch of 0.27 mm). By using the Gimp program [17], the contrast and brightness of each image were manually enhanced so that the pectoral muscle edge could be easily visualized. Then, the pectoral muscle edges were manually drawn by one of the authors (RJF) under the supervision of a radiologist (RAB), without referring to the results of detection by the proposed methods. The zoom option of the Gimp program was used to aid in drawing the edges. The results were printed on paper by using a laser printer with 600 dpi resolution. The pectoral muscle edges of all images were checked by a radiologist (RAB) using the printed images (hardcopy) along with the displayed images (softcopy); the assessment was recorded for a posteriori analysis. (Data files of the manually drawn and automatically detected contours are available from the corresponding author upon request.)

Automatic identification of the pectoral muscle was performed by using down-sampled images of size 256×256 pixels at a resolution of 800 μm. The hand-drawn contours were not down-sampled. The results of detection were transferred to the original full-size images by enlarging twice by a factor of two: the edge pixel detected was always maintained at the upper-left corner of the 2×2 expansion matrix.

The segmentation results related to the edges detected by Method 1 (Hough transform) and Method 2 (Gabor wavelets) were evaluated based upon the number of false-positive (FP) and false-negative (FN) pixels normalized with reference to the corresponding numbers of pixels in the regions demarcated by the manually drawn edges. The reference region for the pectoral muscle was defined as the region contained between the left-hand edge of the mammographic image excluding any blank

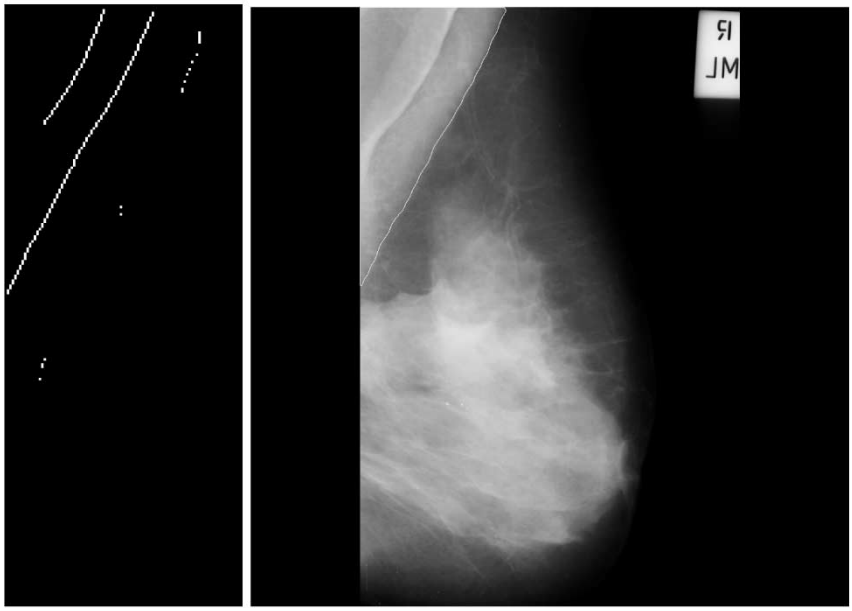

(a) (b)

Fig. 13. Image mdb110 showing the result for the detection of the pectoral muscle in the presence of the pectoralis minor. (a) Edge candidates after the post-processing stage. (b) Final boundary.

portions (that is, the chest wall) and the hand-drawn pectoral muscle edge. An FP pixel was defined as a pixel outside the reference region that was included in the pectoral region segmented. An FN pixel was defined as a pixel in the reference region that was not present within the segmented region.

In addition to the analysis of the pectoral muscle area as explained above, the Hausdorff distance [18] was computed between the hand-drawn pectoral muscle edges and the results of the two proposed methods. Only the pectoral muscle edges within the mammograms were compared; the outer edges at the upper and left-hand boundaries of the images were not used.

VI. Results and Discussion

The results obtained from the segmentation procedures were analyzed according to the protocol described in Section V. A total of 84 images were analyzed; some of the results are provided for the sake of illustration (see Figs. 10–12) and discussion in the following paragraphs. The processing time to perform the identification of the pectoral muscle in the down-sampled 256×256 images was about 0.7 min on the average, using an 850-MHz computer with 512 MB of memory.

The FP and FN average percentages and the corresponding standard deviation values are summarized in Table I. The mean and standard deviation of the Hausdorff distances are also listed in the table. Method 2 (using Gabor filters) resulted in significantly lower FN errors than Method 1 (based upon the Hough transform). In addition, the results of Method 2 have lower Hausdorff distances than those of Method 1. Furthermore, the lower standard deviation of the results of Method 2 also indicate that the Gabor-filter-based method provides more consistent results than the method based upon the Hough transform. This is due to the fact that Method 2 does not use a straight-line model for the pectoral muscle edge. In many mammograms, the pectoral muscle edge curves away from the chest wall toward the middle and lower-half of the images. The results of Method 1 lead to significant FN error in such cases; however, Method 2 is free of such errors: see, for example, Figs. 10 and 11.

From Figs. 10(c) and 11(c), it can be seen that detection using Method 1 results in an underestimated pectoral region due to the limitation imposed by the straight-line hypothesis used to represent the pectoral muscle; this is translated to a high FN rate. The segmentation results of Method 2 [see Figs. 10(d) and 11(d)] are visually much closer to the pectoral muscle edges drawn by the radiologist. The method based on Gabor wavelets and edge-flow propagation removes the limitations of the straight-line hypothesis formulated in our previous work [4] to represent the pectoral muscle edge.

Fig. 12 shows a case where the pectoral muscle appears as a straight line. Even in this case, the result obtained using Gabor wavelets (Method 2) is more accurate than the result obtained using the Hough transform (Method 1). Method 2 provided good results even in cases where the pectoralis minor is present in the mammogram (see Fig. 13).

Fig. 14(b) illustrates an example of underestimation of the pectoral muscle region, giving a high FN rate. In this case, the exact delineation of the pectoral muscle edge is difficult since a section of the pectoral muscle near the chest wall appears mixed with fibro-glandular tissues.

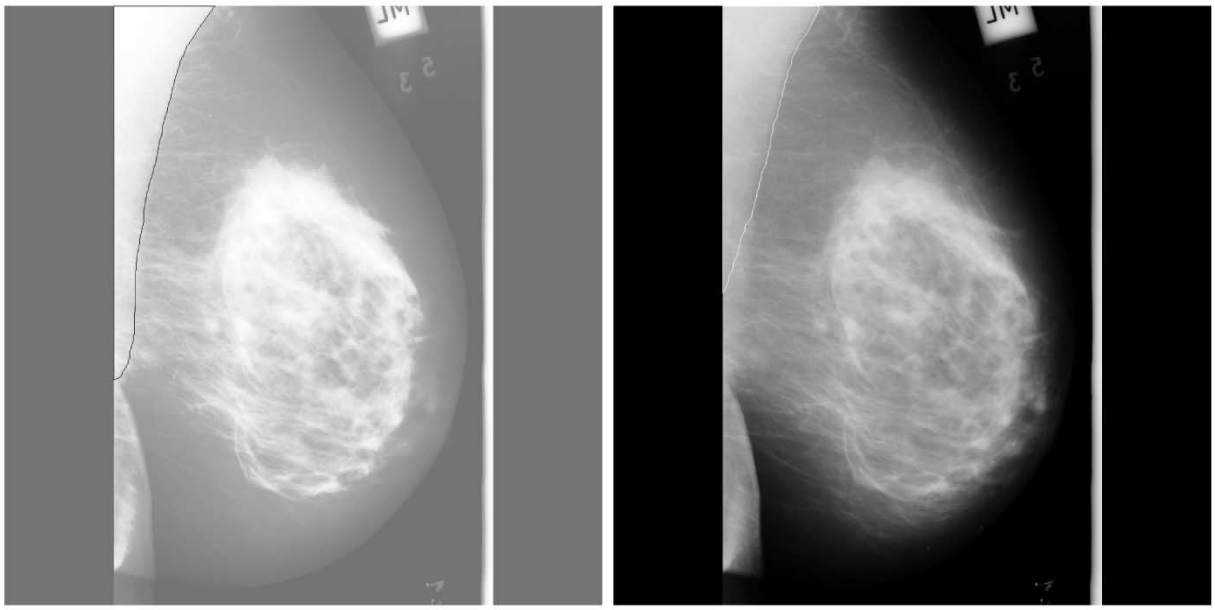

(a) (b)

Fig. 14. (a) Image mdb112 (histogram equalized) with the hand-drawn pectoral muscle edge. (b) The pectoral muscle was underestimated by Method 2, giving a high FN rate of 16.21%. $\mathrm{FP} = 2.33\%$.

VII. Conclusion

We have proposed a new algorithm for automatic segmentation of the pectoral muscle in mammograms. The method, based upon Gabor filters, overcomes the limitation of the straight-line hypothesis imposed by our previous method for the representation of the pectoral muscle. With reference to the number of pixels in manually demarcated pectoral muscle regions, the segmented regions provided by the Gabor-filter-based method resulted in average FP and FN rates of 0.58% and 5.77%, respectively. Furthermore, the results of the Gabor-filter-based method indicated low Hausdorff distances with respect to the hand-drawn pectoral muscle edges, with the mean and standard deviation being 3.84 ± 1.73 mm over 84 images.

According to the opinion of the two radiologists involved in the study, the overall results of the proposed method, applied to 84 images from the Mini-MIAS database [7], are promising for application in the preprocessing stages of computer-aided diagnosis (CAD) systems.

The proposed design of the Gabor filters is based upon parameters related to the human visual system as well as typical characteristics of properly acquired MLO mammograms. Although we have not performed a sensitivity analysis of the results with respect to variations in the parameters of the Gabor filters, we expect the post-processing steps (edge-flow analysis and edge linking) in the proposed method to add robustness to the procedure and reduce the dependence of the final results on the choice of the filter parameters.

The methods proposed have been used as preprocessing steps in segmentation of the fibro-glandular discs in mammograms for the analysis of bilateral asymmetry [19], [8]. The methods should also find use in other applications of medical image analysis, such as improved visualization of catheters during catheterization procedures, and the detection of boundaries of bones in radiographs.

References

[1] M. J. Homer, *Mammographic Interpretation: A Practical Approach*. Boston, MA: McGraw-Hill, 1997.

[2] N. Karssemeijer, "Automated classification of parenchymal patterns in mammograms," *Phys. Med. Biol.*, vol. 43, no. 2, pp. 365–378, 1998.

[3] S. R. Aylward, B. H. Hemminger, and E. D. Pisano, "Mixture modeling for digital mammogram display and analysis," in *Proc. 4th Int. Workshop Digital Mammography*, N. Karssemeijer, M. Thijssen, J. Hendriks, and L. van Erning, Eds., Nijmegen, The Netherlands, June 1998, pp. 305–312.

[4] R. J. Ferrari, R. M. Rangayyan, J. E. L. Desautels, and A. F. Frère, "Segmentation of mammograms: Identification of the skin – air boundary, pectoral muscle, and fibro-glandular disc," in *Proc. 5th Int. Workshop Digital Mammography*, M. J. Yaffe, Ed., Toronto, ON, Canada, June 2000, pp. 573–579.

[5] B. S. Manjunath and W. Y. Ma, "Texture features for browsing and retrieval of image data," *IEEE Trans. Pattern Anal. Machine Intell.*, vol. 18, pp. 837–842, Aug. 1996.

[6] W. K. Pratt, *Digital Image Processing*, 2nd ed. Mountain View, CA: Wiley, 1991.

[7] J. Suckling, J. Parker, D. R. Dance, S. Astley, I. Hutt, C. R. M. Boggis, I. Ricketts, E. Stamatakis, N. Cerneaz, S. L. Kok, P. Taylor, D. Betal, and J. Savage, "The Mammographic Image Analysis Society digital mammogram database," in *Proceedings of the 2nd International Workshop on Digital Mammography*, A.G. Gale, S.M Astley, D.R. Dance, and A.Y Cairns, Eds. York, U.K., July 1994, vol. 1069, Excerpta Medica Int. Congr. Ser., pp. 375–378.

[8] R. J. Ferrari, R. M. Rangayyan, J. E. L. Desaultels, and A. F. Frère, "Analysis of asymmetry in mammograms via directional filtering with Gabor wavelets," *IEEE Trans. Med. Imag.*, vol. 20, pp. 953–964, Sept. 2001.

[9] T. S. Lee, "Image representation using 2–D Gabor wavelets," *IEEE Trans. Pattern Anal. Machine Intell.*, vol. 18, pp. 959–971, Oct. 1996.

[10] S. Mallat, "A theory for multiresolution signal decomposition: The wavelet representation," *IEEE Trans. Pattern Anal. Machine Intell.*, vol. 11, pp. 674–693, July 1989.

[11] B. Jähne, *Digital Image Processing*, 4th ed. San Diego, CA: Springer, 1997.

[12] R. L. De Valois, D. G. Albrecht, and L. G. Thorell, "Spatial frequency selectivity of cells in macaque visual cortex," *Vis. Res.*, vol. 22, pp. 545–559, 1982.

[13] J. G. Daugman, "Uncertainty relation for resolution in space, spatial frequency, and orientation optimized by two-dimensional visual cortical filters," *J. Opt. Soc. Amer.*, vol. 2, no. 7, pp. 1160–1169, 1985.

[14] P. Jones and L. A. Palmer, "An evaluation of the two-dimensional Gabor filter model of simple receptive fields in cat striate cortex," *J. Neurophysiol.*, vol. 58, no. 6, pp. 1233–1258, 1987.

[15] G. Cardenosa, *Breast Imaging Companion*. Philadelphia, PA: Lippincott-Raven, 1997.

[16] W. Y. Ma and B. S. Manjunath, "Edgeflow: A technique for boundary detection and image segmentation," *IEEE Trans. Image Processing*, vol. 9, pp. 1375–1388, Aug. 2000.

[17] P. Mattis and S. Kimball. GIMP – GNU Image Manipulation Program – Version 1.1.17. [Online]. Available: http://www.gimp.org – GNU General Public License – GPL

[18] D. P. Huttenlocher, G. A. Klanderman, and W. J. Rucklidge, "Comparing images using the Hausdorff distance," *IEEE Trans. Pattern Anal. Machine Intell.*, vol. 15, pp. 850–863, Sept. 1993.

[19] R. M. Rangayyan, R. J. Ferrari, J. E. L. Desautels, and A. F. Frère, "Directional analysis of images with Gabor wavelets," in *Proc. XIII Brazilian Symp. Computer Graphics and Image Processing*, Gramado, RS, Brazil, Oct. 2000, pp. 170–177.